High temperature, high pressure hydrogen attack of materials.

A thesis submitted for the degree of Master of Science in
Engineering with Innovation and Entrepreneurship
by

Chigozirim Adanna Ibeabuchi, BEng
Department of Mechanical Engineering
University College London

I, Chigozirim Adanna Ibeabuchi, confirm that the work presented in this thesis is my own. Where information has been derived from other sources, I confirm that this has been indicated in the thesis.

September 2020

Student number: 19065643
Total number of words: 9466

Abstract

The aim of this project was to analyse the susceptibility of superalloys used in the combustion chamber of jet engines to High Temperature Hydrogen Attack or any other hydrogen induced damage. To solve the problem, an extensive literature review was conducted, and a risk assessment was made. The literature review showed that there may be a form of "high temperature" hydrogen embrittlement that affects superalloys. The probability of this high temperature "hydrogen embrittlement" occurring is not definite because when temperatures were raised, the hydrogen embrittlement effects disappeared. However, the finding was still key as it also showed interaction between carbides and trapped hydrogen and this may be the key to understanding if hydrogen attack occurs in superalloys. Also, it was concluded that the stability of some of the carbides may pose a problem as some of the stabilities are unknown. Finally, experiments to test for hydrogen induced damage were designed.

Acknowledgements

I want to thank my supervisor, Dr Wojcik, for his extensive guidance throughout my work on this project. I am extremely grateful for his willingness to answer all my questions and provide clarity on any issues I had. I remain eternally grateful to God for grace to finish this work. I will also like to thank all my family and friends for their unwavering support and prayers.

Table of Contents

1 Introduction

There has been an increasing interest in the use of Hydrogen as a fuel in gas turbines. This is as a result of its extremely small weight and its non-polluting nature when compared to fossil fuels normally used for combustion processes. The increased use of hydrogen as a fuel should lead to a decrease in greenhouse gas emissions which are normally responsible for global warming. There is even the concept of the hydrogen economy where fossil fuels will no longer be used but hydrogen will be the principal energy source. Hydrogen is already being used as a fuel in electric vehicles. The main problem with the use of hydrogen as a fuel is its poor storage capability because of the need for high pressure storage. However, a lot of research is being carried out and this will likely not be an issue in the years to come.

The use of hydrogen in combustion processes seems to be a more common application. Hydrogen is also being considered as a fuel in jet engines. Because of the working conditions of jet engines (high temperature and high pressure), there is need to know how jet engine materials will survive certain extreme conditions. The jet engines (gas turbines) to be considered are made of superalloys. These superalloys could be nickel based, iron based, or cobalt based. They are used because of properties such as high creep strength and high resistance to oxidation and resistance. These superalloys are made up of various phases that have significant effects on their properties. They also undergo heat treatments such as solid solution strengthening and precipitation hardening to enhance their properties.

Hydrogen damages materials in different ways. The most popular way is via hydrogen embrittlement which normally occurs at extremely low temperatures. Another way is via High Temperature Hydrogen Attack. It is a phenomenon which affects steels at extremely high temperatures in surroundings where hydrogen is used. In April 2010, there was an incident that occurred at Tesoro Refinery in Washington, USA. It involved

the rupture of a heat exchanger which was in a catalytic reformer used in the refinery. This heat exchanger which was made of carbon steel had been damaged by high temperature hydrogen attack. It is important to note that not all the heat exchangers present in the Naphtha Hydrotreater unit failed. It was because of only one heat exchanger that the whole incident occurred. This incident of course led to fatal injuries of seven staff that worked in the Tesoro refinery (The US Chemical Safety and Hazard Investigation Board, 2014). If hydrogen is being considered for its use as a fuel in gas turbines, it is important to analyse any safety issues that may occur. Due to the high temperatures used in jet engines, hydrogen embrittlement is not expected to be a likelihood. Hence, there is little research on the susceptibility of superalloys to hydrogen embrittlement at high temperatures.

Carbon and carbides are present in superalloys. Hence, there is a likelihood that these superalloys are susceptible to both Hydrogen Embrittlement and High Temperature Hydrogen Attack. Although there are documented mechanisms for these phenomena, they are not well understood. So, there is still intensive research being carried out on them. There is also not intensive research carried out on the hydrogen damage that may occur in various grades of superalloys. Most of the research focuses on one popular grade of nickel base superalloy (Inconel 718).

This thesis gathers all the literature on superalloys, hydrogen embrittlement, high temperature hydrogen attack, creep, fracture and aims to synthesis this into a logical assessment of whether superalloys (those used in the combustion chamber of jet engines) will be affected by hydrogen. This is a risk assessment project that will check if it will be needful to undertake further research to examine the effect of hydrogen and its possible role in superalloy failure. This thesis tries to fulfil the project aim by carrying out literature survey and having a discussion-based analysis which will analyse the likelihood of hydrogen being harmful to superalloys. It was originally

thought that hydrogen would certainly cause damage to superalloys, but the extent and mechanism of the likely damage was not known. This thesis manages to give an explanation of the severity of some form of hydrogen induced degradation. From the research conducted, it is apparent that there is need for practical experimentation.

The literature survey was supposed to give hints to the type of experiments that should have been carried out. However, the inability to conduct experiments in 2020 only allowed for some of these experiments to be designed but not undertaken. There is a chapter in the thesis that discusses some experiments that can be carried out to test for hydrogen induced damage. There is some discussion on how the damage can be analysed using a non-destructive technique known as the potential drop technique. If the experimental work determines that some form of hydrogen induced damage occurs in superalloys at high temperatures, it is vital that in-situ monitoring of this damage is carried out.

This thesis is divided into nine main chapters. The second chapter will focus on understanding the concept of high temperature hydrogen attack. The third chapter will focus on gas turbines (the parts and the criteria used to select materials for the various components). The fourth chapter will carry out a general survey on superalloys and in particular a thorough survey on the superalloy grades that are likely to be found in the combustion chamber of a jet engine. The fifth chapter will explain the basic concepts of material failure like creep and fracture. The sixth chapter will survey different instances of creep in superalloys. The seventh chapter will do a general survey on hydrogen embrittlement, its mechanisms and the susceptibility of some superalloys to it. The eight chapter will analyse hydrogen induced damage in superalloys based on the surveys carried out. The ninth chapter will describe some experiments that help to detect and monitor hydrogen induced damage in superalloys.

2 High Temperature Hydrogen Attack

2.1 Definition

High Temperature Hydrogen Attack normally affects low alloy steels in environments where hydrogen and high temperatures are used. It usually occurs at temperatures greater than 300°C and pressures greater than 2MPa. High Temperature Hydrogen Attack occurs in different stages and they include: intake or diffusion of hydrogen into metal, decarburisation of steel and intergranular fissuring (Benac and McAndrew, 2012).

2.2 Mechanisms of Attack

There have been quite some studies on the mechanisms that govern high temperature hydrogen attack. (Martin et al., 2017) studied the way in which damage develops in a material during the early stages when bubbles are formed, and cracks are formed as a result of methane formation. They used C-1/2 Mo steel as a sample which had been used in the wall of a depentanizer reboiler. They made some insightful observations and conclusions. It was observed that majority of the cracks formed were intergranular and linked to the inclusions present in the material. There were no noticeable bubbles formed in the sample used in this study. However, there were some bubbles formed along some grain boundaries between ferrite grains and grain boundaries slightly far away from pearlite grains. It was noted that these bubbles were formed on grain boundaries that were 2.5μm from the crack tip in the material. The following conclusions were made concerning the mechanisms that led to hydrogen attack in this material: formation of methane happens at interfaces containing the matrix and inclusions, rate of bubble formation increases as methane formation increases, when bubbles have a particular large size, the grain boundaries that are weak join up to form intergranular cracks. This newly formed intergranular cracks experience a build-up of methane pressure that leads to new bubbles formed

close to the crack tip and finally crack growth increases when these new bubbles are formed close to the crack tip.

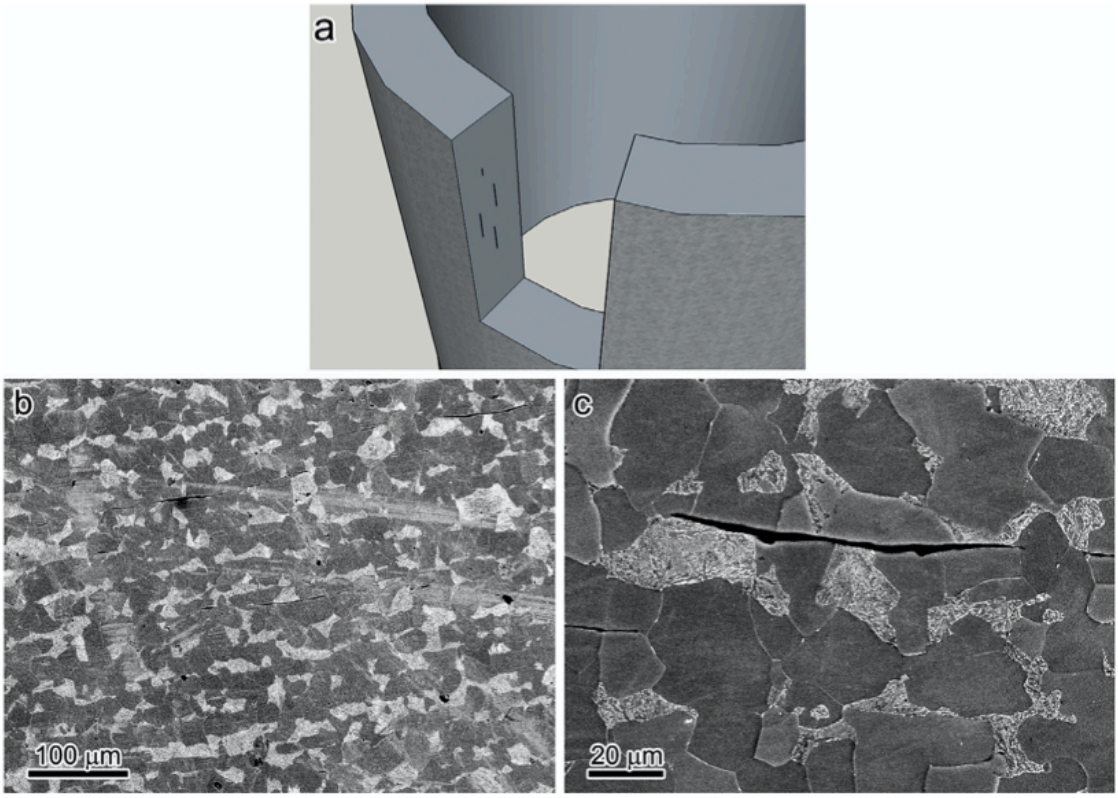

Figure 1 Diagram showing cracking as a result of HTHA in the C-1/2Mo Steel

Source: (Martin et al., 2017)

In order for these bubbles to grow, they must be present along grain boundaries or dislocations. This is because the grain boundaries help in nucleation of bubbles that establish a plane for crack growth. The simple equation that summarises the formation of methane is: $C + 4\,H = CH_4$ (Houbaert and Dilewijns, 1991).

2.3 Cases of HTHA in Carbon Steels and Low Alloy Steels

There have been a lot of studies conducted on the hydrogen attack on various grades of steel. Some of these studies will be highlighted. (Sundararajan and Shewmon, 1980) analysed the kinetics of the hydrogen attack in three different high strength, low alloy steel grades. The steel grades were: High Mn-Cb steel, Armco 787 steel and Mn-Mo-Cb steel. They made the following deductions: the rate of expansion which occurred quite early in the different steel grades was not dependent on time, difference in expansion rate among the different steel grades was in proportion with the carbon activity of the steels and finally the expansion rate of the different steel grades was highly dependent on temperature. When comparisons were made with the 2 ¼ Cr- 1Mo steel, it was seen that it had a higher resistance to hydrogen attack than High Mn-Cb steel because it had a lower carbon activity as a result of the precipitation of M_7C_3 carbide. The High Mn-Cb steel had a higher carbon activity because it had the M_3C carbide which was deemed an unstable carbide.

Another study examined the hydrogen attack of carbon steels. This was conducted by subjecting a sample of SAE 1020 steel to a hydrogen partial pressure of 3.5MPa and a temperature of 525 °C. It was found that after approximately five days of exposure to hydrogen, the tensile properties of the carbon steel deteriorated. It was also found that after the sample was exposed to high pressure hydrogen for 15 days, properties such as the yield strength and elongation-at-fracture decreased rapidly. The part of the samples which were fractured showed the presence of micro void coalescence that would cause ductile rupture. An unusual observation made was that when crack growth experiments were conducted, there were no indications of crack development in the sample. The author translated the lack of crack growth to the absence of crack tips on the grain boundaries of the sample. Finally, the tears and blisters were unevenly dispersed around the sample. Their locations were dependent

on the thickness of a particular part of the sample. These tears and blisters increased the rate of hydrogen attack (Eliezer, 1981).

2.4 Nelson Curves

There are various inspection techniques used for checking if a material has been damaged by hydrogen attack. They are: Advanced Ultrasonic Backscatter Technique (AUBT), Phased Array, In situ metallography and Positive material identification.

However, the Nelson Curves have been designed so that these inspection practices do not even have to happen. The accurate utilisation of the Nelson Curves will help to reduce the probability of HTHA occurring in an environment. The Nelson curves which were developed in 1949 by George Nelson are curves that are intended to showcase safe operating limits for various grades of steels at different temperatures and hydrogen partial pressures. The curves below represent those recommended by the American Petroleum Institute in 2016. There have been several editions and these curves are continually updated as new experiments and discoveries are made. The grades of steel displayed on the Nelson Curves for API 2016 report are: 6.0Cr-0.5Mo Steel, 3.0Cr-0.5Mo Steel, 1.25Cr-0.5Mo Steel, 1.0Cr-0.5Mo Steel, Carbon steel (non-welded or welded with post weld heat treatment) and Carbon steel (welded with no post weld heat treatment). For example, assuming the operating conditions in the industry environment are 2100 psi of Hydrogen partial pressure and 1500 °F, 3.0Cr-1Mo steel will be damaged by hydrogen attack as these figures are above its operating level according to its Nelson curve (American Petroleum Institute, 2016).

.

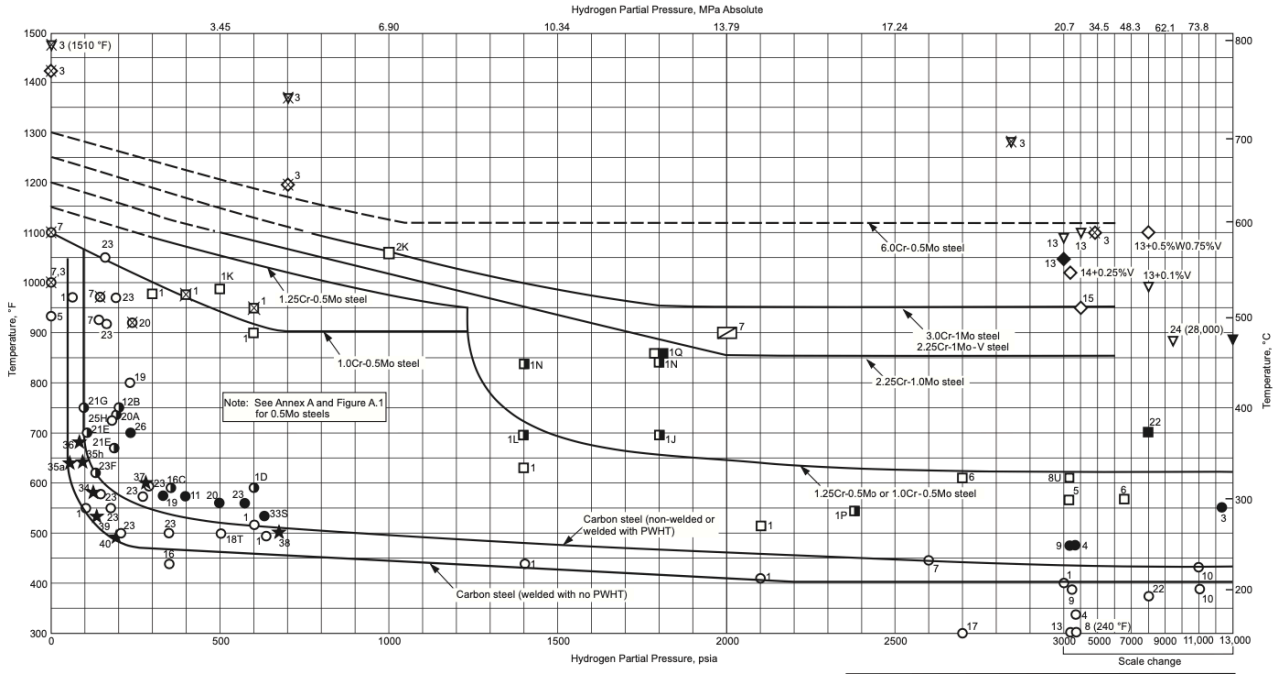

Figure 2 Operating Limits for Steels in Hydrogen Service

Source: (American Petroleum Institute, 2016)

It is important to note that as helpful as the Nelson curve is, it does not consider important factors like creep, the interactions between hydrogen and stress etc.

2.6 Prevention

The susceptibility of a material to hydrogen attack can be reduced or completely prevented. There are a number of modifications to be made to steelmaking to reduce hydrogen attack susceptibility. One common step is the addition of elements that form more stable carbides when processing. Some of these elements are Chromium, Molybdenum, Columbium (now known as Niobium), Vanadium, Titanium etc. When these elements are added, the carbon activity of the steel grade instantly decreases thereby reducing hydrogen attack susceptibility (Sundararajan and Shewmon, 1980).

3 Gas Turbines (Jet Engines)

3.1 Parts of a gas turbine

Gas turbines used for various applications. They can be used as industrial gas turbines to generate power or they can be used as jet engines that provide thrust for aircraft. For the purpose of this thesis, jet engines will be considered. The diagram of a typical jet engine is shown below :

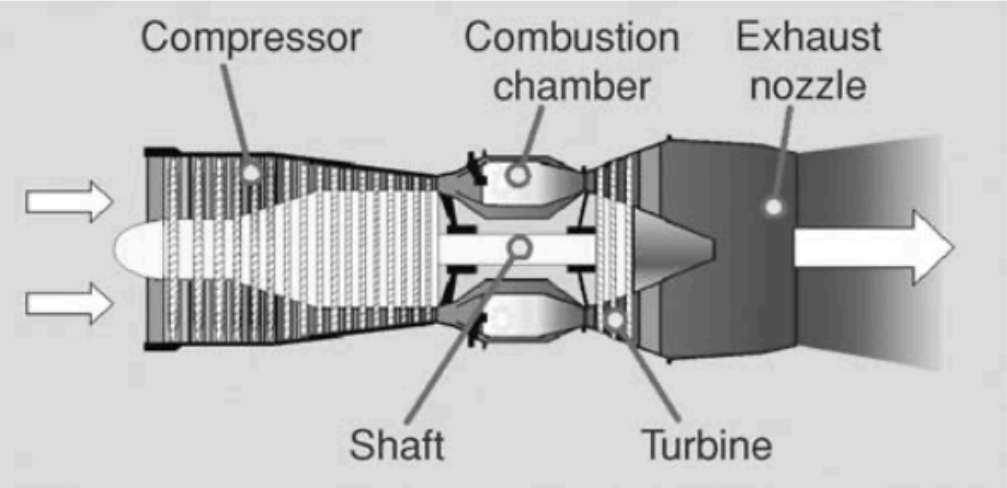

Figure 3 Parts of a Jet Engine

Source: (Reed, 2006, pp.2-49)

There are various configurations of jet engines. They are: turbojet, turboprop and turboshaft. The turbojet configuration produces propulsion from the kinetic energy produced by gas from the exhaust and bypass air which has been pushed around the jet engine core. The turboprop configuration steers the engine propeller as the mechanical load while the turboshaft configuration transfers mechanical power produced to a rotating shaft of the jet engine (Jansohn, 2013, pp.40–319). The different components of a jet engine are: compressor, combustor, turbine, shaft and fan. The compressor which is composed of discs and blades is responsible for squashing the air coming into the engine and raising the pressure of the air. The combustor is responsible for mixing the air from the compressor with fuel and burning up the mixture. The turbine is then responsible for expanding this ignited mixture and releasing the mechanical work that will be used to propel the compressor. The shaft

helps to transfer the torque that will be used to propel the compressor. In the turbofan design, a fan is put in front of the jet engine and acts as a low-pressure compressor (Reed, 2006, pp.2–49).

3.2 Materials Selection for gas turbine components

The type of materials selected to be used in a jet engine will be very key to the performance and life expectancy of that jet engine. In the compressor section, titanium is used because of its large strength to weight proportion. The combustor section of the gas turbine operates at extremely high temperatures from the range of (535°C to 1090°C) and also bears little structural loads, hence, there needs to be a boost in the creep rupture strength without losing the high resistance to oxidation and corrosion. Hence, Nickel-base superalloys are used. Some of these nickel base superalloys are Hastelloy X, Nimonic 263 and Haynes 188. Hastelloy X was the earliest superalloy grade to be used as a result of its high creep strength. Nimonic 263 was the next popular grade and finally the cobalt based superalloy, Haynes 188, is now used as a result of a boost in the turbine firing temperature. It also has a greater creep strength than the other grades. For the discs, they are not exposed to extremely high temperatures. Their design requirements are: high resistance to fatigue and toughness. Inconel 718 is commonly used for the production of the turbine discs (Rao, 2011) and (Geddes, Leon and Huang, 2010, pp.1–24).

4 Superalloys

4.1 Definition

Superalloys as the name implies are high performing alloys that are specifically designed to showcase outstanding mechanical properties and high creep resistance in various components of machines especially when utilised at high temperatures.

4.2 Phases found in Superalloys

Every material has a microstructure. The microstructure of a material is the layout of a material when viewed by a microscope. The microstructure of a material is made up of different phases. These phases are uniform parts of the system that have similar physical and chemical properties (Callister and Rethwisch, 2018, pp.253–300). Phases exist in the microstructure of superalloys and some of them are: the gamma phase, the gamma prime phase, carbide and boride phases etc. Some of these phases will be explained below according to research from (Donachie and Donachie, 2002, pp.25–39) and (Krishna, 2010):

- The Gamma Phase (γ): This phase is made up of a face centred cubic (FCC) structure. This phase possesses a variety of elements. Some of these elements are: chromium, molybdenum, cobalt etc. This phase creates a continuous matrix phase where all other phases which may be present dwell in.
- The Gamma Prime Phase (γ'): This is the main strengthening phase in a lot of nickel and iron-nickel base superalloys. This phase also has a face centred cubic (fcc)- ordered $L1_2$ crystal structure. The compounds normally precipitated by this phase are: Ni_3Al and Ni_3Ti.
- The Gamma Prime Phase (γ''): This phase is more common in superalloys such as Inconel 718. This is a phase with a body centred tetragonal (bct)- DO_{22} crystal structure that produces Ni_3Nb precipitates. It acts as the main strengthening phase and precipitates formed are particles which are shaped like discs. One drawback of this phase is that its solvus temperature is smaller than that of the gamma prime phase.
- Eta phase (η): This phase is found in superalloys that have large titanium and aluminium proportions after the superalloys have been exposed for very long periods of time. It has a hexagonal close packed (DO_{24}) crystal structure. The compound normally precipitated by this phase is Ni_3Ti.

- Carbide Phase: This phase is made up of mixed carbides in the form: MC, M_6C, $M_{23}C_6$ and M_7C_3. All of these carbides have face centred cubic crystal structures except for the MC and M_7C_3 phases which have cubic and hexagonal crystal structures respectively. The MC phase is a primary phase which is sometimes irregularly shaped that produces precipitates like TiC, HfC and NbC. The $M_{23}C_6$ phase is formed during low temperatures and is normally precipitated along grain boundaries and precipitates compounds like $Cr_{23}C_6$ and $(Cr,Mo,Fe,W)_{23}C_6$.

  The M_6C phase is normally formed at higher temperatures than the $M_{23}C_6$ phase. The M_6C phase which is normally distributed around various parts of the microstructure precipitates compounds like: Fe_3Mo_3C, Fe_3W_3C, Fe_3Nb_3C and Fe_4W_2C. The M_7C_3 phase is normally detected at temperatures greater than 1000°C. The compound mainly precipitated by this phase is Cr_7C_3. The carbide phases undergo transformations at various temperatures. From 750°C to 1000°C, the primary carbide (MC) can transform to a secondary carbide i.e. MC + γ-----> $M_{23}C_6$ + γ'. It can be seen that this reaction leads to the precipitation of the gamma prime phase which is a strengthening phase intended to enhance the creep strength of the superalloy. Similar phase transformations that may occur to the carbides are: MC + γ-----> M_6C + γ' and M_6C + M′ -----> $M_{23}C_6$ + M′′. The latter reaction is as a result of long-term exposure. Most of these phase transformations depend on the superalloy and its alloying elements.
- TCP Phases: These phases comprise of the mu phase (μ), laves phase and the sigma phase (σ). All of these phases are formed at extremely high temperatures and could be damaging to the creep strength of the superalloys. These phases sometimes help in the initiation of cracks in superalloys.

It is important to note that the explanations of the phases above may not apply to very grade of superalloy. Some slight differences in phase behaviour may be observed.

4.3 Classifications of Superalloys

Superalloys are commonly divided into three groups. These groups are:

- Nickel-base superalloys
- Iron-base superalloys
- Cobalt-base superalloys

Nickel-base Superalloys

For the purpose of this this research, nickel-base superalloys will be the principal superalloys used for investigation. They are the superalloys that have the largest amount of strengths at extremely high temperatures. Some examples are: Inconel 718, Waspaloy, CMSX-4 etc (Geddes, Leon and Huang, 2010, pp.1–24).

Iron-base Superalloys

This group of superalloys as the name implies have a large percentage of iron in them (typically from 29-67%). They are derived from steels with a crystalline structure that is austenitic. They are also machined with more ease when compared to the other superalloy classes as a result of low strength properties that they possess. The typical examples of iron-base superalloys are N-155 Incoloy 800 and A-286 (Youssef, 2016, p.31).

Cobalt-base Superalloys

These superalloys generally have a higher percentage of cobalt in them (from 35-67%). They are known for being more resistant to hot corrosion, thermal fatigue and more weldable that nickel-base superalloys. However, nickel-base superalloys showcase more strength than them. They are not used a lot because they are very

expensive. Typical examples of cobalt-base superalloys are Haynes 188 and Haynes 25 (Youssef, 2016, pp.39–40).

4.4 Strengthening of Superalloys

Strengthening treatments are very important to improve a whole lot of properties such as creep resistance in superalloys.

Solid Solution Strengthening

This has to do with the improvement of matrix strength of a particular metal. This is achieved by the addition of various soluble elements used for alloying. This strengthening method leads to malformation in the atomic lattice of the material which ultimately causes a halt in the movement of dislocations in the matrix. This strengthening mechanism causes the material's stacking fault energy to decrease. The stacking fault energy is the energy generated as a result of irregularities which are present in the stacking order of atoms in a crystal lattice. A small stacking fault energy implies that the dislocations present in the lattice will not easily modify their directions. Solid solution strengthening gives strength for temperatures not greater than 815°C. Some elements used for solid solution strengthening are: Titanium, Molybdenum, Tungsten, Chromium etc. (Geddes, Leon and Huang, 2010, pp.1–24).

Precipitation Hardening

This is a strengthening mechanism that involves the enhancement of creep strength in superalloys. It is achieved by the inclusion of elements like aluminium, titanium and niobium. These inclusions are not exactly soluble in the matrix of the superalloy and for a reduction in temperature, solubility is decreased which creates gamma prime or gamma prime prime precipitates. The gamma prime (γ') precipitates are normally compounds like $Ni_3(Ti,Al)$ while the gamma prime prime (γ'') comprises of compounds like Ni_3Nb. These precipitates help to prevent the motion of dislocations inside the matrix. There are certain determinants that show that whatever

precipitation hardening treatment that was carried out was successful. These determinants are: size of particle, energy of antiphase boundary when (γ', γ'') precipitates are present, strain in coherence between γ and (γ', γ'') precipitates and finally (γ', γ'') precipitates volume fraction (Geddes, Leon and Huang, 2010, pp.1–24).

4.5 Hastelloy X and Nimonic 263 in Detail

Two common grades of superalloys found in combustion chambers are Hastelloy X and Nimonic 263. It is necessary to know the phases present in these superalloys as they could have a huge influence on their properties.

Nimonic 263

This is a precipitation hardened wrought nickel-base superalloy. It is commonly used in the combustion chamber of jet engines. The typical chemical composition of this superalloy in % is shown below (Special Metals Corporation, 2004):

Element	Composition (%)
C	0.04 - 0.08
Si	0.40
Mn	0.60
S	0.007
Ag	0.0005
Al	0.60
B	0.005
Bi	0.0001
Co	19.0 - 21.0
Cr	19.0 - 21.0
Cu	0.20
Fe	0.70
Mo	5.6 -6.1

Pb	0.0020
Ti	1.9 - 2.4
Ni	Bal

Table 1 Table showing Composition of Nimonic 263

This alloy goes through two heat treatments: solid solution strengthening and precipitation hardening. As with every material, depending on heat treatment methods and conditions such as temperature, various phases are found in Nimonic 263. The phases will be described according to the research carried out by (Zhao, Ravikumar and Beltran, 2001). For the purpose of the research, the Nimonic 263 sample was subject to certain heat treatments. The samples were solution annealed at 1150 ◦ C, water quenched and finally subjected to precipitation hardening at different temperatures (750 ◦ C , 850 ◦ C and 900 ◦ C). Using transmission electron microscopy (TEM) and scanning electron microscopy (SEM), the microstructure and phases present in the superalloy were observed at various temperatures. The phases found in this superalloy are:

- Gamma - prime phase (γ'): This phase is made up of $(Ni,Co)_3(Ti,Al)$ precipitates with an ordered face centred cubic structure. In this study, this phase was mainly found at temperatures less than 900°c.
- Eta phase (η): This phase was made up of $Ni,Co)_3Ti$ precipitates with a hexagonal ($D0_{24}$) crystal structure. This phase formed at the expense of the gamma prime phase after long annealing periods.
- $M_{23}C_6$ phase : This phase was made up of $Cr_{23}C_6$ precipitates with a face centred cubic structure. Most of these precipitates were found along grain boundaries at temperatures of 750°C, 850°C and 900°C when the annealing period was 50 hours. They were the majority carbide precipitates found across grain boundaries.

- MC phase: This phase was made up (Ti, Mo) C precipitates with a face centred cubic structure. This phase was found at all heat treatment temperatures when the annealing period was 50 hours. This phase was also found at grain boundaries.

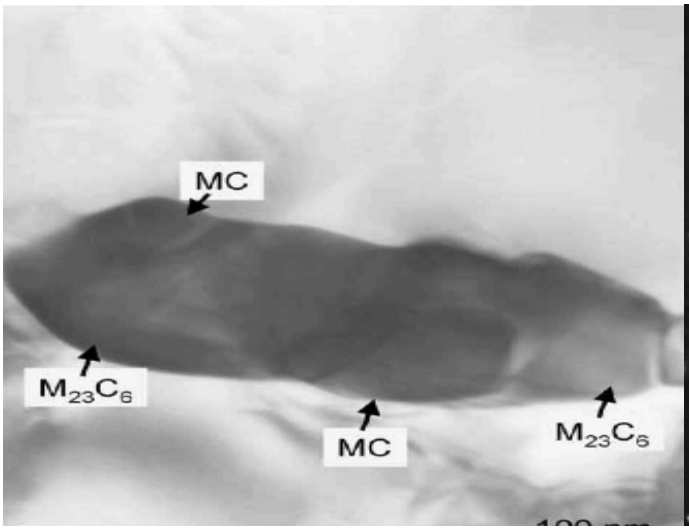

Figure 5 Grain Boundary Precipitates when sample was heat treated at 900°C for 50 hours

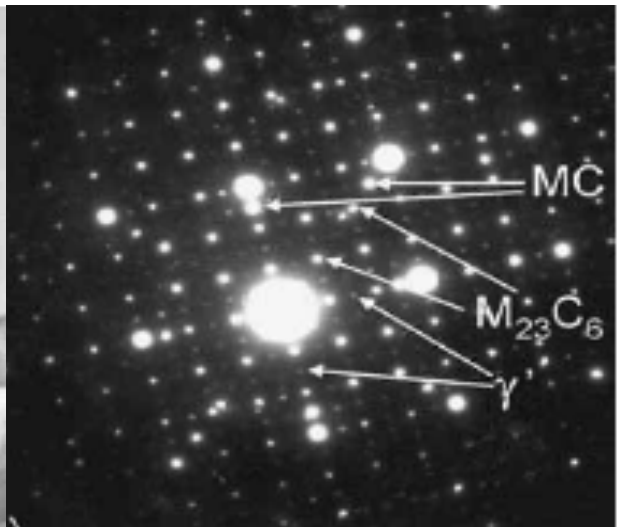

Figure 4 Precipitates formed when sample was heat treated at 750°C for 50 hours

Source: (Zhao, Ravikumar and Beltran, 2001)

Hastelloy X

This is also a wrought nickel-base superalloy. It is commonly solid solution strengthened and also found in the combustor of jet engines. The typical chemical composition off this superalloy in % is shown in the table below (Haynes International, 2015):

Element	Composition (%)
Ni	47 balance
Cr	22
Fe	18
Mo	9
Co	1.5

W	0.6
C	0.1
Mn	1 max
Si	1 max
B	0.008 max
Nb	0.5 max
Al	0.5 max
Ti	0.5 max

Table 2 Table showing Composition of Hatelloy X

(Zhao, Larsen and Ravikumar, 2000) carried out a study using transmission electron microscopy (TEM) to study how different phases precipitated in Hastelloy X. The already solution annealed samples were subject to another solution annealing at 1150 ° C, water quenched and finally subjected to precipitation hardening at different temperatures (750 ° C, 850 ° C and 900 ° C). The precipitation annealing was carried out at these temperatures for 26 hours and 100 hours. The following phases were present:

- M_6C: This phase was present at all temperatures when the heat treatment was for both 26 and 100 hours. This phase was also present in twin boundaries that existed in the microstructure at all temperatures and heat treatment periods. This phase was abundant in Molybdenum, Chromium and Nickel.
- $M_{23}C_6$ phase: This phase appeared as intragranular precipitates when the precipitation annealing was carried out at 750°C for 26 hours. As with Nimonic 263, this phase was also abundant in Chromium. At a much higher temperature and short heat treatment periods (950°C and 26hours), this phase was not present but when the heat treatment period extended to 100 hours small precipitates were observed.
- σ phase: This phase appeared as small precipitates at 850°C when the sample was heat treated for 26 hours. This phase was mainly made up of Chromium.

- μ phase: This phase was mainly made up of Molybdenum and started appearing when the precipitation annealing was carried out at 850°C for 26 hours. These precipitates had stacking faults. For this same heat treatment temperature but for a longer period i.e. 100 hours, this phase could be seen but was not easily distinguishable from the other phases present in the superalloy.

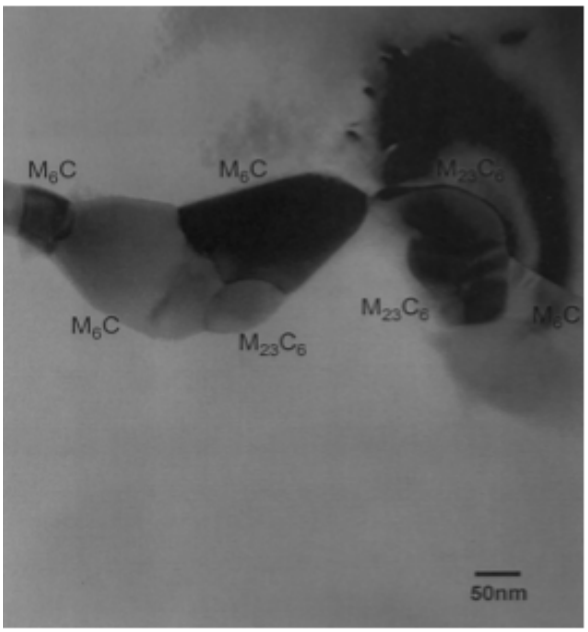

Figure 6 Grain boundary precipitates when sample was heat treated at 750°C for 26 hours.

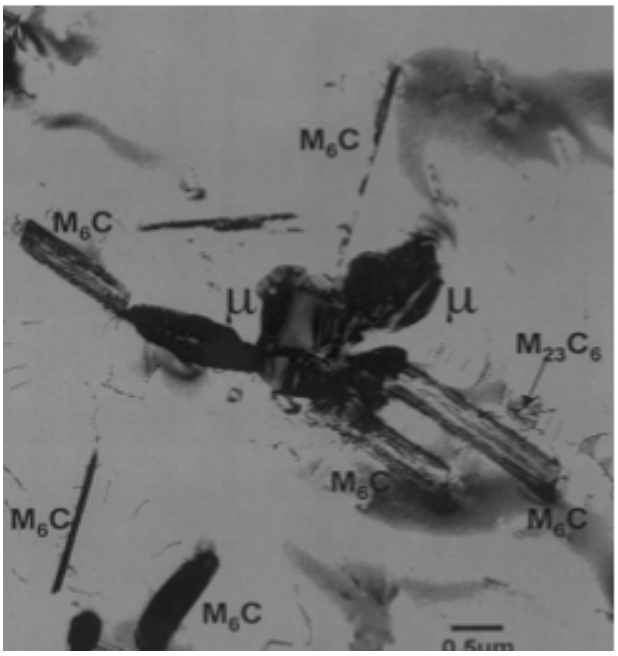

Figure 7 Precipitates formed when sample was heat treated at 850°C for 100 hours.

Source: (Zhao, Larsen and Ravikumar, 2000)

5 Brief Overview on Material Failure

5.1 Fracture

5.1.1 Definition and Types

Fracture is a process that occurs when a body is split into two or more parts as a result of static stress and temperatures that are small when compared to the melting temperature of that particular material. Fracture is caused by fatigue which is failure as a result of recurring loading. For fracture to occur, cracks must be formed and grow in the material.

There are two main types of fracture and they are ductile and brittle fracture:

- Ductile Fracture: This is a type of fracture that is associated with a considerable plastic deformation of material and large energy absorption.
- Brittle Fracture: This type of fracture is characterised by having no plastic deformation and a small amount of energy absorption.

There are also types of fracture that describe the direction of crack propagation in the material. Transgranular fracture indicates that the cracks move through the grains in the material while intergranular fracture means the cracks growing across grain boundaries (Callister and Rethwisch, 2018, pp.253–300).

5.2 Creep

5.2.1 Definition

Creep can be described as a type of time-dependent deformation that occurs to all types of materials that are operated at high temperature levels and are subject to all sorts of mechanical stresses at these high temperatures. The temperature at which metals become more susceptible to it is when these metals are operating at a temperature greater than 2/5 of their melting temperature i.e. $0.4T_m$. The creep equation that describes steady state creep is given below:

$$\dot{\varepsilon}=\frac{C\sigma^m}{d^b}e^{\frac{-Q}{kT}}$$

$\dot{\boldsymbol{\varepsilon}}$=creep strain rate, C=a variable that depends on the material, $\boldsymbol{\sigma}$=stress applied to material, m & b=exponents associated with the creep mechanism in play, d=grain size of material, Q=activation energy of creep mechanism, k= Boltzmann's constant, T=Temperature in Kelvin (Dowling, 2019, pp.802–821).

5.2.2 The Creep Curve

The creep curve consists of various regions: area illustrating primary creep, secondary creep and tertiary creep. These regions describe the creep behaviour of a material at different time intervals (Callister and Rethwisch, 2018, pp.253–300).

- Primary Creep: This is also referred to as transient creep. From the figure below, it can be seen that this particular creep is characterised by a creep rate that is steadily decreasing. This characteristic implies that creep resistance in the particular material is increasing hence it is very hard for the material to be deformed.
- Secondary Creep: This is also referred to as steady-state creep. At this stage, the creep rate is uniform. This stage of creep takes place for the longest period of time.
- Tertiary Creep: This stage of creep is characterised by having the creep strain rate increase as the stress applied to the material increases. This stage leads to the final failure of the particular material.

The diagram below shows the different stages of creep occurring at different periods:

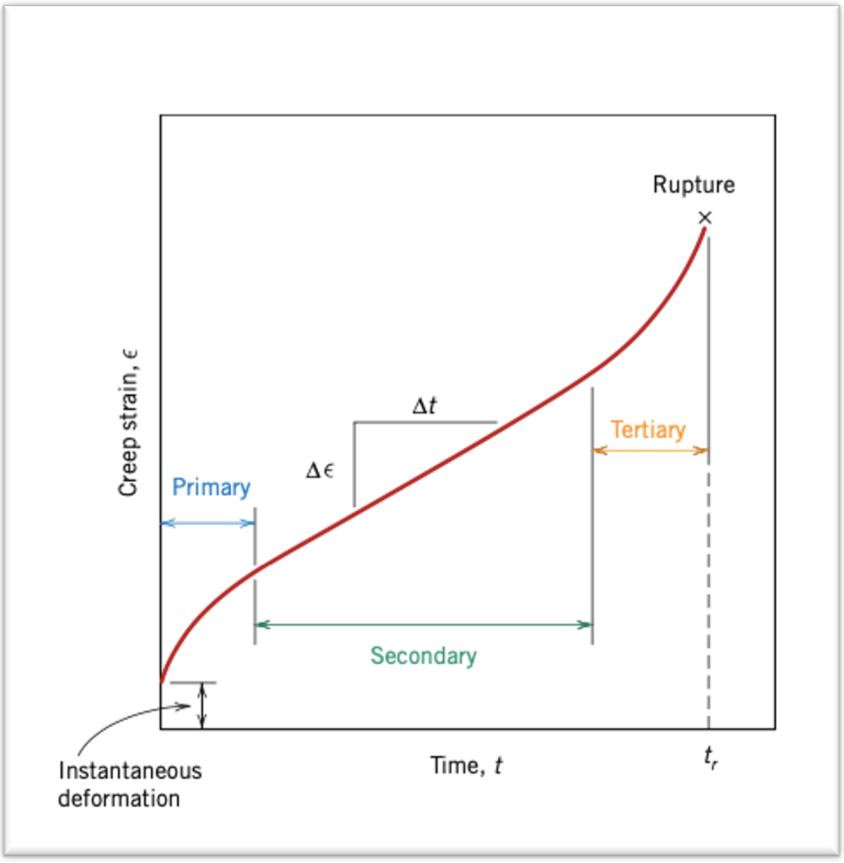

Figure 8 Typical Creep Curve

Source: (Callister and Rethwisch, 2018, pp.253–300)

5.2.3 Creep Mechanisms

There are two main creep mechanisms and they are: Dislocation creep and Diffusion Creep. When stress is applied to a material, the creep in that material is controlled by the motion of the dislocations present in that material. This creep mechanism is referred to as dislocation creep. This creep mechanism which is also referred to as power-law creep normally occurs when large stresses are applied to the material. This mechanism also comes into play when median temperatures are used, and the diffusional flow is minimum. For this creep mechanism, the m in the creep equation can be from values (3-8) while b has a value of 0.

Diffusional creep normally involves low stresses applied and extremely high temperatures. It has to do with the motion of holes in a crystal lattice. Diffusional creep has to do with the motion of holes in the crystal lattice of the material. This motion occurs because the holes being formed are close to grain boundaries that are roughly normal to the stress applied to the material. This unequal distribution of holes or vacancies leads to the diffusion of these holes to areas with lower concentrations. Diffusional creep has two common mechanisms. They are: Nabarro-Herring creep and Coble creep. Nabarro-Herring creep involves the motion of these holes through the crystal lattice of this material. For this mechanism, the strain rate is in proportion with the stress and a reciprocal of the grain size. Hence, m has a value of 1 and b has a value of 2. For Coble creep, the holes move across the grain boundaries and the relationship between the stress and strain rate is similar to that of Nabarro-Herring creep. However, for this case b has a value of 3 (Dowling, 2019, pp.802–821).

6 Creep in Superalloys

Although superalloys were created on the basis of having high creep strengths, they are still very susceptible to creep. The susceptibility of superalloys to creep damage will be reviewed in this section.

A study analysed the creep behaviour of the Nimonic 263 superalloy over the temperature range of 600°C- 950°C. At a temperature of 600°C and stresses that ranged from 680MPa to 750MPa, it could be observed from the creep curves that this superalloy underwent a large transient creep stage. After some time, the superalloy experienced fracture and the tertiary stage of creep appeared. At temperatures ranging from 700 to 800°C, the stresses applied to the specimen (180MPa, 225MPa and 545MPa) were lower than the yield stress of the material. At this stage, the primary creep obtained was smaller than that obtained when the temperature was 600°C. The tertiary creep stage was dominant at this temperature and stresses. When the temperature was increased to 900°C and 950°C with low applied stresses of 31,36,50 and 70MPa, the primary creep stage was deemed insignificant and at applied stresses of 31 and 36MPa, the tertiary creep stage was followed by the secondary creep stage. Then, the tertiary creep stage appeared again, and fracture occurred (Maldini, Angella and Lupinc, 2007).

Another study used the NR6 superalloy commonly used in turbine disks to understand the creep behaviour of this material when subjected to different heat treatment methods. This superalloy grade is being considered because of its function in the turbine discs which are also hot components of a gas turbine. The three heat treatment methods used gave this material three different microstructures. The first microstructure was obtained as a result of over ageing heat treatment, the second microstructure was obtained as a result of cooling at a slow rate of 4 $^{\circ}C\ min^{-1}$ while the third microstructure was obtained by using a subsolvus heat treatment which

lasted for 120 hours and finally a supersolvus heat treatment. The grain size produced by using the third heat treatment method was 50μM while that of the first and second heat treatment methods were 28μM and 25μM respectively.

The grain boundary morphology of the first and third heat treatment methods was straight except for that of the second heat treatment method which gave a serrated grain boundary morphology. The creep test was carried out at 700°C with an applied stress of 700Mpa. Two creep tests were carried out: creep rupture and interrupted creep tests. For the creep rupture test, it showed that the specimen with the overaged microstructure produced the highest minimum creep rate ($7.7.\times 10^{-9}$ $^{s-1}$) and lowest time to rupture (512 hours). On the other hand, the specimen produced by the third heat treatment method which had a microstructure with coarse grains had the lowest minimum creep rate ($1.3.\times 10^{-9}$ $^{s-1}$) and a higher rupture time (699 hours).

The interrupted creep test had some significant findings which will be briefly summarised. With regards to the characterisation of local deformation, it showed that the deformation of the specimen with the coarse grain microstructure was more heterogeneously distributed when compared with specimens that had overaged and serrated grain boundary microstructures. In regard to grain boundary sliding amplitude, the original microstructure had the highest GBS amplitude (116nm). The average grain boundary sliding amplitude of the other microstructures are: Overaged- 63nm, Serrated grain boundary – 52nm and Coarse grains – 80nm. it is important to note that out of all of these three microstructures, the one with the overaged microstructure had tertiary γ' precipitates that were fully dissolved. This implied that dislocation motion was easier in this microstructure which led it to have the highest creep rate. The specimen with the serrated grain boundary microstructure showed more homogenous intragranular deformation and the lowest grain boundary sliding amplitude. For the coarse grain microstructure, intragranular deformation is

more heterogenous which means that although grain boundary sliding has a higher amplitude, its contribution to overall strain is the lowest when compared to other microstructures (0.11) (Thibault et al., 2013).

Another study carried out fatigue-crack-growth experiments on three different nickel-based superalloys: Haynes R-41, Haynes 230 and Hastelloy X. Before carrying out the tests to check crack growth, all of the alloy specimens were precracked to a size of 1.27mm. The temperatures in which these crack growth experiments ranged from 760°C to 927°C. The fatigue-crack crack growth experiments were carried out with the use of a triangular waveform with frequency- 0.333Hz and load ratio of 0.05. The tests showed that without hold time at a temperature of 816°C , Hastelloy X had the highest crack growth rate while that of the other two superalloys were similar. With a hold time of two minutes, Haynes R-41 superalloy had the highest creep-fatigue resistance while that of Hastelloy-x had the lowest creep-fatigue resistance. Since the Hastelloy X is of main concern in this research, only its fracture modes will be discussed. In regard to the fracture modes, it was observed that at 816°C in Hastelloy X, with a hold time of two minutes, the fracture mode transformed from transgranular to intergranular. At 927°C, the fracture mode was more visibly intergranular and also had a higher rate of crack growth (Lee et al., 2008).

7 Hydrogen Embrittlement

7.1 Definition

Hydrogen Embrittlement which is also referred to as Hydrogen assisted cracking is a dangerous phenomenon that affects different types of metals at low temperatures. It involves the damage of a particular metal grade after they have been exposed to gaseous hydrogen. It happens when hydrogen diffuses into a metal, becomes trapped in it and produces stress that helps to spread cracks in the metal thereby embrittling the entire metal. There are various factors that determine if a particular

material is more susceptible to hydrogen embrittlement. These factors are: material microstructure, pressure, temperature, heat treatment that may have been undergone by this material, strength of material and hydrogen concentration (Dwivedi and Vishwakarma, 2018).

7.2 Mechanisms

There are certain mechanisms that govern hydrogen embrittlement. They are: Hydrogen enhanced decohesion mechanism (HEDE), Hydrogen enhanced local plasticity model (HELP), Absorption-induced dislocation emission (AIDE), Hydrogen Enhanced Macroscopic Ductility (HEMP), Hydrogen Changed micro-fracture mode (HAM), Decohesive hydrogen fracture (DHFO, Mixed fracture (MF) and Hydrogen assisted micro void coalescence (HDMC). The three main mechanisms will be summarised below as explained by (Dwivedi and Vishwakarma, 2018); (Robertson et al., 2015); (Lynch, 2012); (Rudomilova, Prošek and Luckeneder, 2018).

- Hydrogen Enhanced Decohesion Mechanism (HEDE): This is a mechanism that leads to the reduction in binding strength of a particular material around the crack tip of this material after exposure to hydrogen atom. This causes the inter-atomic bond strength in this material to be greatly reduced too. The surface energy of the material shrinks as a result of this making the material more susceptible to fracture.
- Hydrogen Enhanced Localised Plasticity (HELP): This mechanism involves the accumulation of hydrogen atoms close to the crack tip of the material. This accumulation leads to reduction in dislocation motion resistance thereby increasing the dislocation mobility susceptibility. The increase in dislocation motion leads to more sites that act as drivers for plastic deformation.
- Absorption-induced dislocation emission (AIDE): The main concept of this mechanism is that dislocation motion is accelerated by hydrogen adsorbed on

the crack tip exterior that causes the reduction in interatomic bonds in the metal. This mechanism combines concepts from the HELP and HEDE mechanism. This mechanism causes the growth of cracks. The trails in which these cracks may be present may either be intergranular or transgranular. This is dependent on the location where dislocation emission and void evolution happened with ease.

7.3 Hydrogen Embrittlement in Superalloys

Some research has been carried out on the susceptibility of certain superalloys to Hydrogen Embrittlement. The findings of some of these studies will be discussed. One research investigated the susceptibility of a Nickel based superalloy (Ni -16Mo -7Cr) that is commonly used in molten salt reactors. To carry out this investigation, this particular superalloy with a very high nickel content was solution annealed. This superalloy was exposed to hydrogen via hydrogen charging using a current density of 160mA cm^{-2} in the presence of a solution of Sulphuric acid. The superalloy was charged for different time periods: 24,48,96 and 144 hours. After charging, the superalloy was tested for hydrogen embrittlement using tensile testing. Using SEM analysis, it could be seen that without hydrogen pre- charging, the fracture mode of the superalloy was ductile while that with hydrogen charging showed brittle fracture attributes on the surface of the superalloy and ductile fracture attributes on the inside part of the superalloy. It was also observed that as the charging time increased, the extent of brittle fracture also grew, and the superalloy's ultimate tensile strength reduced. Cracks could be observed on the grain boundary and slip traces could be seen on the surface of the superalloy that had been charged with hydrogen. At a particular hydrogen concentration, the bonding strength of the grain boundary decreased, and nano-voids nucleated on the grain boundary of the superalloy. These nano-voids could then lead to intergranular fracture (Han et al., 2018). For this

particular nickel-based superalloy, hydrogen embrittlement is certain because intergranular fracture was observed.

A study investigated the susceptibility of Inconel 600, Hastelloy X and Nickel to hydrogen embrittlement. To carry out this investigation, the specimens of these alloys were subject to heating at a temperature of 1200°C for one hour and water cooling. They also underwent some other heat treatments which involved ageing from 600-900°C for 100 hours. After the heat treatments, the specimens were exposed to hydrogen in an autoclave at a temperature of 450°C for twenty hours. This was carried out at pressures ranging from 1-30MPa. The Hastelloy X superalloy is the alloy of concern here as it is the only alloy relevant to this research. It was found that no significant hydrogen embrittlement was observed in the smooth Hastelloy X sample. The effects of the ageing treatment carried out at 900°C on hydrogen embrittlement susceptibility was noted. In Hastelloy X, it was seen that as the ageing time 900°C increased to up to 100 hours, the ultimate tensile strength and elongation of the Hastelloy X specimen reduced significantly. It was also observed that for ageing treatments that were carried out below 600°C, the deterioration of Hastelloy X exposed to hydrogen was not visible. However, for the specimens aged above 700°C which were also exposed to hydrogen, the ultimate tensile strength and elongation of the Hastelloy X specimen decreased. It was finally concluded that the hydrogen embrittlement susceptibility of Hastelloy X increased when subjected to ageing treatments above 700°C. One key observation made was that when pure nickel was dehydrogenated, it did not regain its original tensile strength and elongation. The Hydrogen Embrittlement susceptibility of Hastelloy X increased because ageing at higher temperatures led to precipitation of carbides in matrix and on grain boundaries (Hasegawa and Osawa, 1981).

7.4 Difference between Hydrogen Embrittlement and High Temperature Hydrogen Attack

The major difference between Hydrogen Embrittlement and Hydrogen attack is the temperatures at which they occur. Hydrogen Embrittlement tends to occur at lower temperatures while Hydrogen attack occurs at extremely high temperatures. In Hydrogen embrittlement, internal pressure is generated by hydrogen while in hydrogen attack, the internal pressure is generated by methane. Another major difference is the mechanisms. Hydrogen Embrittlement is governed by mechanisms such as Hydrogen Enhanced Localised Plasticity (HELP) and Hydrogen Enhanced Decohesion (HEDE) which have already been explained. None of these mechanisms govern the high temperature, hydrogen attack of carbon and low alloy steels.

8 Analysis of Hydrogen Induced Damage in Nickel Base Superalloys

"High Temperature" Hydrogen Embrittlement Susceptibility Analysis

Unlike Steels, Hydrogen Embrittlement in Superalloys occurs at a much wider range of temperatures. (Hasegawa and Osawa,1981) have been able to prove this as previously explained. They tried to investigate if Hastelloy X was going to be affected by hydrogen embrittlement at ageing temperatures ranging from 600°C to 900°C. It was seen that at low temperatures (600°C), this was not the case but from 700°C, the specimen was affected by Hydrogen Embrittlement. Hydrogenation caused a reduction in tensile strength and elongation of the specimen that had been charged with hydrogen. This is expected as the carbide precipitates in Hastelloy X which have been mentioned in this report were noticed to have started precipitating from temperatures of 750°C. The carbide/matrix interface can be said to act as hydrogen traps. Some of these traps can be reversible or irreversible. In the superalloys analysed in this study (Hastelloy X and Nimonic 263), these same $M_{23}C_6$ precipitates were found on grain boundaries. This means that these grain boundaries may have a

way of trapping hydrogen. These trapped hydrogen atoms will either remain in the carbide/matrix interface for a long time or diffuse.

Cold working is a process used after welding in materials like steels. The process normally involves the generation of hydrogen. The generation of this hydrogen normally makes it easy for hydrogen to be trapped in Steels. The jet engine is not going to be in service all the time. There are times when it will be out of service. So, the "cold-working" effect may be able to come into play here. When the turbine is no longer in use and is gradually cooling, there may be some residue hydrogen gas left in the combustion chamber. This residue hydrogen gas may react with the carbon in the carbide/matrix interface of the superalloy.

As the ageing temperature increased, the precipitates coarsened. So, there is a risk of fewer trap sites if extremely high temperatures are used. This is because as the precipitates grew bigger, their surface area to volume ratio reduced hence the decrease in the number of trap sites.

Effect of Carbide Stability

As shown with hydrogen attack in low alloy steels, the stability of the carbide is very key to ensuring the formation of methane. In Hastelloy x, the principal carbides present in the microstructure are: M_6C and $M_{23}C_6$. M_6C is rich in molybdenum while $M_{23}C_6$ is rich in chromium. The stability of M_6C cannot really be determined as there is no experimental work based on the stability of $(Mo,Cr,Ni)_6C$. However, there is extensive work on the stability of $Cr_{23}C_6$. The free energy of formation of a compound plays a huge role in determining the stability of that compound. From the Ellingham diagram shown in figure 9, it can be seen that at low temperatures, the free energy of formation of $Cr_{23}C_6$ is about -70kJ/gram-atom. At higher temperatures, this value reduces to approximately -80kJ/gram-atom. The change in free energy of formation

at high temperatures is not so much. However, it can be said that this compound is more likely to be unstable at high temperatures because the free energy of formation is closer to being more positive than it is to being more negative. This is not certain of course. It is also an established fact that the more positive the free energy of formation is, the more unstable the compound becomes.

For Nimonic 263, the main carbides present in the superalloy are MC and $M_{23}C_6$. MC is rich in Titanium and Molybdenum while $M_{23}C_6$ is rich in chromium. MC is a mixed carbide. If two separate compounds are being analysed (MoC and TiC), it can be seen from the diagram below that MoC is highly unstable at low temperatures and starts to become stable at extremely high temperatures. However, TiC seems to be very stable at low and high temperatures. However, the stability of MC carbides is still not certain.

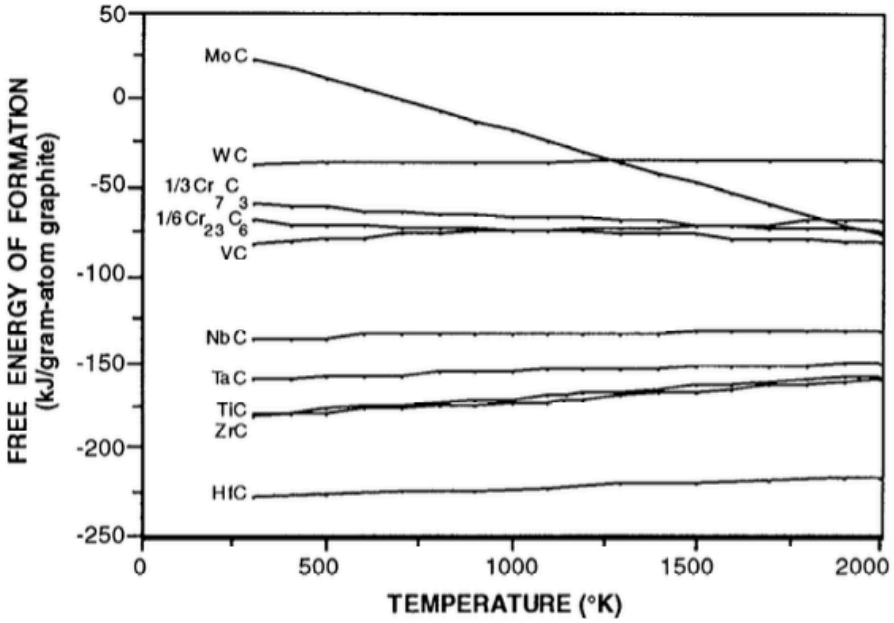

Figure 9 Ellingham Diagram showing the free energy of formation for carbides at different temperatures

Source: (Nell and Grant, 1992)

Summary

It has been seen that in Hastelloy X, carbide matrix interfaces act as trap sites for hydrogen. The trapping of this hydrogen led to likely embrittlement of the superalloy. This finding is important because this embrittlement occurred at a temperature higher than the temperature range for hydrogen embrittlement. So, the phenomenon observed can be said to be "High Temperature" Hydrogen Embrittlement. It is not certain that hydrogen attack occurs because no information has been given on the formation of methane. The definite thing is that hydrogen and the carbides have some sort of interaction.

If the stability of carbides is considered, it can be said that from the Ellingham diagram, $Cr_{23}C_6$ ($M_{23}C_6$) which is commonly precipitated at grain boundaries is fairly stable. However, the stability of mixed carbides like M_6C and MC which are also precipitated by Hastelloy X and Nimonic 263 respectively cannot be determined as there is not a lot of information regarding their stability. The pressure of methane as a factor that influences hydrogen attack cannot be considered because it is uncertain if methane is formed at high temperatures in superalloys.

9 Proposed Experiments to detect HTHA Susceptibility

There is a lot of doubt based on the explanations given about the susceptibility of Nimonic 263 and Hastelloy X to high temperature hydrogen attack. Hence, it is important to start somewhere by designing experiments that will test for their susceptibility to hydrogen induced damage at elevated temperatures and also examine effects of this hydrogen damage.

1st Proposed Experiment

The first experiment to consider will be to investigate the effect of hydrogen damage on the creep strength of the material. These experiments will involve using the

specimens of superalloys used in the combustion section in the jet engine. The superalloys to be analysed will be: Hastelloy X, Nimonic 263.

The first proposed experiment is based off the experiment conducted by (Yokogawa et al., 1989). This involves analysing the effect of high temperature, high pressure hydrogen in a creep rupture vessel similar to that designed by (Yokogawa, Fukuyama and Kudo, 1982). The specimens will need to be machined into appropriate gauge lengths and they will also need to be heat treated. Their heat treatment is as follows:

- Hastelloy X: Solution annealing at 1175°C and aging at 800°C for eight hours.
- Nimonic 263: Solution annealing at 1150°C and aging at 800°C for two hours.

The vessel used for testing will be described in the next few sentences. It is basically a high-pressure vessel embedded within the normal apparatus used for creep rupture tests. High temperatures will be supplied by the furnace. Four thermocouples will be used. One will be used to administer the test temperature while the other three will be used to compute the temperature during the experiment. The time of fracture will be documented by a timer which halts immediately fracture occurs. Hydrogen or argon gas will be let into the vessel via a pipe that is connected to the counter chamber.

These creep rupture tests will be performed in both hydrogen and argon at particular pressures. Some modifications need to be made. One is that the temperature will not be fixed. The other one is that the test will occur at different hydrogen concentrations. The creep rupture test will take place at temperatures of 500°C, 700°C and 900°C.

The graphs to be derived from this experiment are:

- Graph of Creep rate vs Hydrogen Content (ppm) for different applied temperatures and stresses.
- Graph of Strain vs Time for different applied temperatures, stresses and hydrogen concentration.
- Graph of Stress vs Rupture Time.

2nd Proposed Experiment

The experiment conducted by (Hasegawa and Osawa, 1981), only tested for hydrogen embrittlement susceptibility of Hastelloy X. This new experiment will adopt some aspects of their experiment and test the hydrogen embrittlement susceptibility of Hastelloy X, Nimonic 263 and pure nickel samples. The same heat treatment methods done in the first experiment will be applied here. However, in this case the specimens will be heated to temperatures of 500°C, 700°C , 900°C and 1000°C for a long period of time (24- 150 hours). After heating, they will be exposed to hydrogen gas at a certain pressure. Tensile tests will then be carried out to measure change in tensile strength and elongation. To see if dehydrogenation has an effect on hydrogen embrittlement susceptibility, the hydrogen will be removed from all the specimens at certain temperatures (not yet determined) in a vacuum for a certain time period. The main graphs to be derived from this experiment are:

- Graph showing elongation and tensile strength in specimens with and without hydrogen.
- Graph of Elongation and tensile strength versus dehydrogenation time.

3rd Proposed Experiment

One of the main features that will be prominent as a result of high temperature hydrogen attack is the presence of voids. Therefore, tests must be conducted to detect the presence of any voids in the damaged material. The potential drop test is a very useful in detecting and monitoring crack growth in a material. The potential drop technique follows the law that as the resistance across a body increases, the length of cracks present will also increase. There are two types of the potential drop technique: Direct current potential drop (DCPD) and Alternating current potential drop (ACPD). The ACPD method is normally preferred over the DCPD method because of some concerns with measurement accuracy. The ACPD method allows for the incorporation of the skin effect. The skin effect is when the alternating current

flows in zones that are close to the surface of the conducting material. The depth of penetration helps to determine how big or small the skin effect is. The depth of penetration is given by the formula below:

$$\Delta = \sqrt{\frac{\rho}{\pi \cdot \mu \cdot f}}$$

$$\rho = resistivity, f = frequency\ and\ \mu = magnetic\ permeability.$$

The impedance across the conductor is highly dependent on all the parameters listed above. Due to the skin effect, the relationship between the impedance and crack growth is linear. This makes measurements easier (Venkatsubramanian and Unvala, 1984). Hence, while this method is preferred to DCPD. For the experiment that will be carried out, the potential drop across a combustion chamber will be measured in-situ. This measurement may take place over the course of 1-2 years. The expected setup of the experiment is shown below:

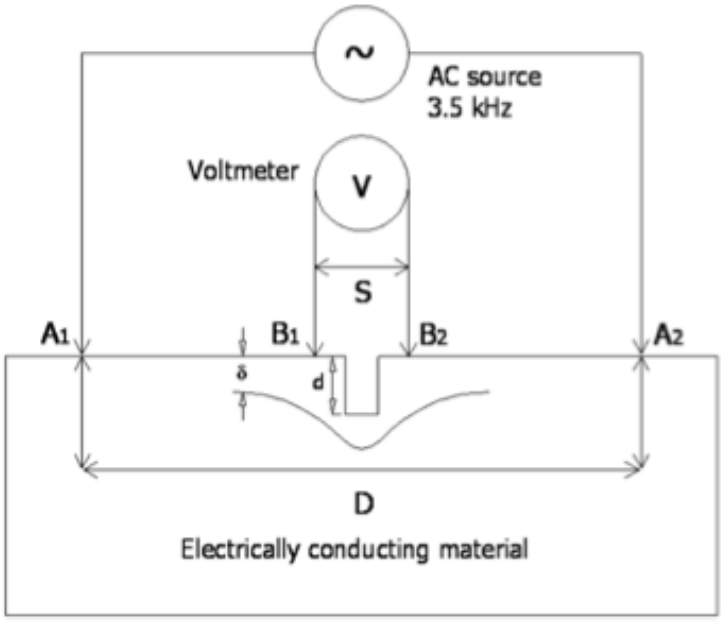

Figure 10 Proposed Setup of ACPD Method

Source: (Raja et al., 2010)

Alternating current will be introduced to the combustion chamber via probes A1 and A2. B1 and B2 are probes which will be used to measure the potential difference

across two points in the combustion chamber. The crack depth can then be measured using the formula below:

$$d = \frac{s}{2}\left(\frac{V_c}{V_o} - 1\right)$$

s= distance between electrodes B1 and B2.

V_o=ks=potential between B1 and B2 in regions without cracks. Where, k= $\frac{I \cdot \rho}{A}$. I= current, p= resistivity and A= area.

V_c= k (2d+s) = potential gotten as a result of placement along cracks with a depth of d (Raja et al., 2010b).

10 Conclusion

The aim of this project was to investigate the susceptibility of materials utilised in the combustion chamber of the jet engine to high temperature hydrogen attack. This was carried out by understanding the nature of the materials used in the combustion chamber of the jet engine, studying the phases present in their microstructure, understanding basic concepts of fracture, creep and hydrogen embrittlement. One paper provided a ground-breaking result that had not been observed before. One of the superalloy grades (Hastelloy X), became susceptible to hydrogen embrittlement at a high temperature (700°C). However, when the temperature was increased to 800°C, the tensile strength and elongation started increasing. This was also an important observation. It was concluded that the carbide/matrix interfaces play a role in the hydrogen trapping, but it was not certain if methane was formed at those regions.

When carbide stability was considered, only one of the carbides ($M_{23}C_6$) could have their stability estimated with the use of an Ellingham diagram. The stability of the other carbides (M_6C and MC) could not easily be estimated as they are mixed carbides. It was therefore summarised that some form of high temperature hydrogen damage may happen to superalloys, but it is not certain that this damage is Hydrogen

attack. So, some experiments were designed to test for the influence of hydrogen on the creep strength of the superalloys and another one known as the potential drop technique was designed to monitor a combustion chamber in situ for crack growth over an extended period of time. It is also recommended that further experiments and research should be carried out to study the relationship between precipitate coarsening at high temperatures and hydrogen trapping capability, the stability of mixed carbides and the likelihood of methane formation when hydrogen is trapped by carbides at high temperatures.

11 Bibliography

American Petroleum Institute (2016). *Steels for Hydrogen Service at Elevated Temperatures and Pressures in Petroleum Refineries and Petrochemical Plants*. [online] *global.ihs.com*, Washington, DC: American Petroleum Institute, pp.2–14. Available at: https://global.ihs.com/doc_detail.cfm?document_name=API%20RP%20941&item_s_key=00010704 [Accessed Feb. 2020].

Benac, D.J. and McAndrew, P. (2012). Reducing the Risk of High Temperature Hydrogen Attack (HTHA) Failures. *Journal of Failure Analysis and Prevention*, [online] 12(6), pp.624–627. Available at: https://link.springer.com/content/pdf/10.1007/s11668-012-9605-x.pdf [Accessed 11 Aug. 2020].

Callister, W.D. and Rethwisch, D.G. (2018). *Materials science and engineering : an introduction*. 9th ed. Hoboken, Nj: Wiley, pp.253–300.

Donachie, M.J. and Donachie, S.J. (2002). *Superalloys : a technical guide*. 2nd ed. Materials Park, Oh: ASM International, pp.25–39.

Dowling, N.E. (2019). *Mechanical behavior of materials : engineering methods for deformation, fracture, and fatigue*. 4th ed. Hoboken, Nj: Pearson Education, Inc, pp.802–821.

Dwivedi, S.K. and Vishwakarma, M. (2018). Hydrogen embrittlement in different materials: A review. *International Journal of Hydrogen Energy*, [online] 43(46), pp.21603–21616. Available at: https://reader.elsevier.com/reader/sd/pii/S0360319918331306?token=90F736B3CC18C 7F648FE4667E9E5982B9830D306F2128BBAD5286BA45C6A3DDB771228E6287096F6300E7DF1 50611735 [Accessed 1 Aug. 2020].

Eliezer, D. (1981). High-temperature hydrogen attack of carbon steel. *Journal of Materials Science*, [online] 16(11), pp.2962–2966. Available at: https://link.springer.com/content/pdf/10.1007/BF00540300.pdf [Accessed 28 Aug. 2020].

Geddes, B., Leon, H. and Huang, X. (2010). *Superalloys : alloying and performance*. Materials Park, Ohio: Asm International, pp.1–24.

Han, F., He, S., Liu, M. and Zhou, X.T. (2018). Hydrogen embrittlement susceptibility of a Ni-16Mo-7Cr base superalloy. *Materials Science and Engineering: A*, [online] 733, pp.291–298. Available at: https://www.sciencedirect.com/science/article/pii/S0921509318310116 [Accessed 5 Aug. 2020].

Hasegawa, M. and Osawa, M. (1981). Hydrogen Damage of Nickel-base Heat Resistant Alloys. *Transactions of the Iron and Steel Institute of Japan*, [online] 21(1), pp.25–31. Available at: https://www.jstage.jst.go.jp/article/isijinternational1966/21/1/21_1_25/_pdf/-char/en [Accessed 31 Jul. 2020].

Haynes International (2015). *Nominal Composition*. [online] Haynesintl.com. Available at: https://www.haynesintl.com/alloys/alloy-portfolio_/High-temperature-Alloys/HASTELLOY-X-alloy/HASTELLOY-X-principal-features.aspx [Accessed 3 Aug. 2020].

Houbaert, Y. and Dilewijns, J. (1991). Identification and quantification of hydrogen attack. *International Journal of Pressure Vessels and Piping*, [online] 46(1), pp.113–124. Available at: https://reader.elsevier.com/reader/sd/pii/030801619190072A?token=2B84B92799978779BBA0EFD502EDF2EF49E8DD825DB44B8E3A084CA3E46FAF0FF3DA12F3043B4CEA0D799AF0E67A7C6A [Accessed 23 Aug. 2020].

Jansohn, P. (2013). *Modern gas turbine systems : high efficiency, low emission, fuel flexible power generation*. Oxford: Woodhead Publishing, pp.40–319.

Krishna, R. (2010). *Microstructural Investigation of Alloys Used for Power Generation Industries*. PhD Thesis. pp.1–212.

Lee, S.Y., Liaw, P.K., Lu, Y.L., Fielden, D., Pike, L.M. and Klarstrom, D.L. (2008). ELEVATED-TEMPERATURE CREEP-FATIGUE CRACK-GROWTH BEHAVIOR OF NICKEL- BASED HAYNES® R-41, HAYNES® 230® and HASTELLOY® X AllOYS. *The Minerals, Materials and Metals Society*, [online] pp.509–514. Available at: https://www.tms.org/Superalloys/10.7449/2008/Superalloys_2008_509_514.pdf [Accessed 2020 Aug. 1AD].

Lynch, S. (2012). Hydrogen embrittlement phenomena and mechanisms. *Corrosion Reviews*, 30(3–4), pp.105–123.

Maldini, M., Angella, G. and Lupinc, V. (2007). Analysis of creep curves of a nickel base superalloy in a wide stress/temperature range. *Materials Science and Engineering: A*, [online] 462(1–2), pp.436–440. Available at: https://www.sciencedirect.com/science/article/pii/S092150930601923X?via%3Dihub [Accessed 31 Jul. 2020].

Martin, M.L., Dadfarnia, M., Orwig, S., Moore, D. and Sofronis, P. (2017). A microstructure-based mechanism of cracking in high temperature hydrogen attack. *Acta Materialia*, [online] 140, pp.300–304. Available at: https://pdf.sciencedirectassets.com/271635 [Accessed 14 Aug. 2020].

Nell, J.M. and Grant, N.J. (1992). Multiphase Strengthened Nickel Base Superalloys Containing Refractory Carbide Dispersions. *Superalloys 1992 (Seventh International Symposium)*, [online] pp.114–121. Available at: https://www.semanticscholar.org/paper/Multiphase-Strengthened-Nickel-Base-Superalloys-Nell-Grant/c8c1afd622c967bb5e9a63634ee221266335e5ab [Accessed 4 Sep. 2020].

Raja, M., Mahadevan, S., Bhagi, P.C.R. and Behera, S.P. (2010a). *Schematic description of the ACPD technique.* Available at: https://iopscience-iop-org.libproxy.ucl.ac.uk/article/10.1088/0957-0233/21/10/105702/pdf [Accessed 12 Sep. 2020].

Raja, M.K., Mahadevan, S., Rao, B.P.C., Behera, S.P., Jayakumar, T. and Raj, B. (2010b). Influence of crack length on crack depth measurement by an alternating current potential drop technique. *Measurement Science and Technology*, [online] 21(10), p.105702. Available at: https://iopscience-iop-org.libproxy.ucl.ac.uk/article/10.1088/0957-0233/21/10/105702/pdf [Accessed 12 Sep. 2020].

Rao, N. (2011). Materials for Gas Turbines – An Overview. In: E. Benini, ed., *Advances in Gas Turbine Technology*. [online] InTech, pp.293–316. Available at: http://www.intechopen.com/books/advances-in-gas-turbine-technology/materials-for-gas-turbines-an-overview [Accessed Aug. 2020].

Reed, R.C. (2006). *The Superalloys : fundamentals and applications.* New York: Cambridge University Press, pp.2–49.

Robertson, I.M., Sofronis, P., Nagao, A., Martin, M.L., Wang, S., Gross, D.W. and Nygren, K.E. (2015). Hydrogen Embrittlement Understood. *Metallurgical and Materials Transactions B*, 46(3), pp.1085–1103.

Rudomilova, D., Prošek, T. and Luckeneder, G. (2018). Techniques for investigation of hydrogen embrittlement of advanced high strength steels. *Corrosion Reviews*, 36(5), pp.413–434.

Special Metals Corporation (2004). *NIMONIC ® alloy 263*. [online] *specialmetals.com*, pp.1–11. Available at: https://www.specialmetals.com/assets/smc/documents/alloys/nimonic/nimonic-alloy-263.pdf [Accessed 3 Aug. 2020].

Sundararajan, G. and Shewmon, P.G. (1980). The hydrogen attack of HSLA steels. *Metallurgical Transactions A*, [online] 11(3), pp.509–516. Available at: https://link.springer.com/content/pdf/10.1007/BF02654574.pdf [Accessed 30 Aug. 2020].

The US Chemical Safety and Hazard Investigation Board (2014). *Catastrophic Rupture of Heat Exchanger (Seven Fatalities)*. Washington,DC.: The US Chemical Safety and Hazard Investigation Board, pp.1–36.

Thibault, K., Locq, D., Caron, P., Boivin, D., Renollet, Y. and Bréchet, Y. (2013). Influence of microstructure on local intra- and intergranular deformations during creep of a nickel-based superalloy at 700°C. *Materials Science and Engineering: A*, [online] 588, pp.14–21. Available at: https://www-sciencedirect-com.libproxy.ucl.ac.uk/science/article/pii/S0921509313009908#t0020 [Accessed 29 Jul. 2020].

Venkatsubramanian, T.V. and Unvala, B.A. (1984). An AC potential drop system for monitoring crack length. *Journal of Physics E: Scientific Instruments*, [online] 17(9), pp.765–771. Available at: https://iopscience-iop-org.libproxy.ucl.ac.uk/article/10.1088/0022-3735/17/9/012/pdf [Accessed 11 Sep. 2020].

Yokogawa, K., Fukuyama, S. and Kudo, K. (1982). Apparatus for creep rupture testing in high-pressure hydrogen at elevated temperatures. *Review of Scientific Instruments*, 53(1), pp.86–89.

Yokogawa, K., Fukuyama, S., Kudo, K. and Shewmon, P.G. (1989). Effect of hydrogen attack on tensile and creep properties of low carbon steel. *International Journal of Pressure Vessels and Piping*, 37(5), pp.365–385.

Youssef, H.A. (2016a). *Machining of stainless steels and super alloys : traditional and nontraditional techniques*. [online] Chichester, West Sussex, United Kingdom: Wiley, p.31. Available at: https://onlinelibrary.wiley.com/doi/book/10.1002/9781118919514 [Accessed 2 Aug. 2020].

Youssef, H.A. (2016b). *Machining of stainless steels and super alloys : traditional and nontraditional techniques*. [online] Chichester, West Sussex, United Kingdom: Wiley, pp.39–40. Available at: https://onlinelibrary.wiley.com/doi/book/10.1002/9781118919514 [Accessed 2 Aug. 2020].

Zhao, J.-C., Larsen, M. and Ravikumar, V. (2000). Phase precipitation and time–temperature-transformation diagram of Hastelloy X. *Materials Science and Engineering: A*, [online] 293(1–2), pp.112–119. Available at: https://www.sciencedirect.com/science/article/pii/S0921509300010492 [Accessed 5 Aug. 2020].

Zhao, J.-C., Ravikumar, V. and Beltran, A.M. (2001). Phase precipitation and phase stability in nimonic 263. *Metallurgical and Materials Transactions A*, [online] 32(6), pp.1271–1282. Available at: https://link.springer.com/content/pdf/10.1007/s11661-001-0217-4.pdf [Accessed 3 Aug. 2020].